DYNAMICS AND AERODYNAMIC CONTROL OF A CROSS-TRACK TETHER SATELLITE SYSTEM

Stefano Aliberti[(1)], **Marco B. Quadrelli**[(2)], **Marcello Romano**[(1)]

[(1)]*Politecnico di Torino, Corso Duca Degli Abruzzi, 24, 10129, Turin, Italy, [stefano.aliberti@polito.it, marcello.romano@polito.it]*
[(2)]*Jet Propulsion Laboratory, California Institute of Technology, 4800 Oak Grove Drive, Pasadena, CA, 91109-8099 – U.S.A. marco.b.quadrelli@jpl.nasa.gov*

ABSTRACT

The objective of this paper is to analyze the dynamics and control strategy of a new type of formation flying architecture, enabling unprecedented space mission capabilities.
We propose a tether satellite system composed of two satellites, flying in LEO, connected by a linear tether, maintained in tension along the cross-track direction (perpendicular to the motion and radial directions). A three-dimensional multibody model was developed, by writing the equations of relative dynamics in an orbiting reference frame. The dynamic model was linearized and an optimal LQR controller was introduced. The linear control law was validated by simulating its application on the full system model, demonstrating the possibility of stabilizing the system by using a unidirectional and constant force. Aerodynamic surfaces were then inserted into the model so as to generate the required force. Finally, the proposed aerodynamic stabilization approach was compared to a gyroscopic stabilization alternative strategy.

1 INTRODUCTION

Space tethers are cables that mechanically connect two or more satellites. They have a variety of applications, ranging from propulsion to momentum exchange [3]. Since 1974, when this concept was first introduced, several studies have investigated the potential of using tethers in space [9]. Among these, the use of tether for formation flying appears to be very convenient. By introducing a tether that connects formation elements in a radial direction, i.e., perpendicular to the Earth's surface, it is possible to take vantage of the stabilizing effect of Earth's gravity gradient.

Nevertheless, it would be also convenient to stabilize these systems in different configurations, so as to expand the range of possible applications.

The use of environmental effects for free-flying spacecraft control is not new to the literature. Several studies have been performed on aerodynamic and solar radiation pressure control. Examples of these applications can be found in [7] where control strategies based on aerodynamic drag to perform rendezvous maneuvers are introduced, in [10] where an aerodynamic attitude stabilization is analysed or in [2] where a possible attitude control based on solar radiation pressure is studied.

This paper, by following the original idea presented in [12], introduces for the first time, to the best knowledge of the authors, a control based on aerodynamic forces for stabilizing a tethered system.

This consists of the introduction of aerodynamic surfaces, placed on the satellites at the ends of the tether, which stabilize a tether system that spans along cross-track direction, i.e., aligned with the direction of the angular momentum of the orbit.

Obtaining a large-aperture oriented in the cross-track direction could enable unique remote sensing missions. For instance, by using synthetic aperture radar techniques, it is possible to obtain the same performance of a large antenna through the use of several antenna elements that sample the signal in space. A system of satellites extending in the cross-track direction allows particularly convenient sampling for earth observation applications, in fact, the greater the beseline and number of satellites in the cross-track direction is, the more directional and accurate the measurement obtained will be [11].

The paper is organised as follows. Section 2 introduces the mathematical model of the system dynamics and equations of motion. Section 3 introduces the mathematical model of the aerodynamic forces generated by the control surfaces. Section 4 introduces the process used to synthesize an LQR controller based on the linearized model of the system. Section 5 introduces the numerical data used in the simulations. Section 6 shows the results of the simulations. In Section 7, the proposed architecture is compared with a tethered system stabilized by gyroscopic effects. Finally, Section 8 summarizes the results, emphasizing advantages and challenges of the proposed system.

2 KINEMATICS AND DYNAMICS

This section introduces the models and equations used to simulate the non-linear dynamics of a tether satellite system in low Earth orbit. Initially, the relative dynamics equation used to describe the evolution of the system with respect to an orbiting reference frame is analyzed, and then the models used for external perturbations and the simulation of tether dynamics are introduced. Finally, the complete ODE system used to analyse the behaviour of the system is defined.
The following notation is used:

- Unit vectors are represented in lowercase characters with a hat: $\hat{a}$
- Vectors are represented in lowercase, underlined characters: $\underline{a}$
- Matrix of components of a vector $\underline{v}$ in the Cartesian Coordinate System A is defined by bold character and superscript letter : $\mathbf{v}^A$
- Matrices are represented in uppercase characters with brackets: [A]

In this study, two Cartesian Coordinate System (CCS) are used. The first one is the Earth Centered Inertial (ECI) CCS. This consists in a quasi-inertial CCS centered in the Earth's center E and having coordinates axes identified by the following unit vectors:

- $\hat{e}_1$ is pointed towards the Vernal Equinox;
- $\hat{e}_3$ is pointed towards the celestial North Pole;
- $\hat{e}_2$ completes the right-hand triad $\hat{e}_2 = \hat{e}_3 \times \hat{e}_1$

The second CCS is the Local Vertical-Local Horizontal (LVLH). This CCS is centered in the instantaneous position of a orbiting satellite O (real or virtual), called Chief, and has coordinate axes identified by the following unit vectors:

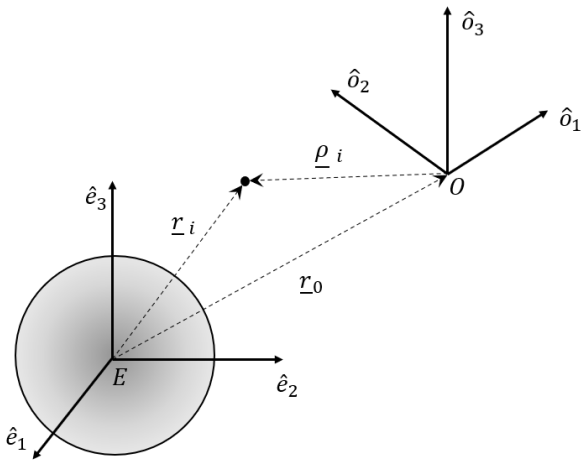

Figure 1: Representation of ECI and LVLH Cartesian Coordinates Systems.

- $\hat{o}_1 = \underline{r}_0/\|\underline{r}_0\|$ is pointed toward the instantaneous radial direction;
- $\hat{o}_3 = (\underline{r}_0 \times \dot{\underline{r}}_0)/\|\underline{r}_0 \times \dot{\underline{r}}_0\|$ is pointed toward the angular momentum vector (cross-track);
- $\hat{o}_2$ completes the right-hand triad $\hat{o}_2 = \hat{o}_3 \times \hat{o}_1$ (along-track).

Where $\underline{r}_0$ denotes the position vector of the center of the orbiting reference frame, and the dot is used to indicate the time derivatives with respect to the inertial frame.
The equation of the dynamics are here obtained by following the same procedure described by Pastori et al. [13]. By denoting by $\underline{r}_i$ the position vector of the i-th satellite, it yields:

$$\underline{r}_i = \underline{r}_0 + \underline{\rho}_i \tag{1}$$

where $\underline{\rho}_i$ indicates the relative position of the i-th satellite with respect to the chief satellite.
The Cartesian Coordinate System introduced and the vector described in the previous equation are visualized in Fig. 1.
At this point it is necessary to take into account that the LVLH frame is not inertial, being in rotation with respect to the ECI frame. By taking the time derivative with respect to the inertial frame, terms caused by the apparent accelerations resulting from the relative rotation of the two systems appear:

$$\ddot{\underline{r}}_i - \ddot{\underline{r}}_0 = \ddot{\underline{\rho}}_i \equiv \overset{\circ\circ}{\underline{\rho}}_i + \dot{\underline{\Omega}} \times \underline{\rho}_i + \underline{\Omega} \times \underline{\Omega} \times \underline{\rho}_i + 2\underline{\Omega} \times \overset{\circ}{\underline{\rho}}_i \tag{2}$$

Where $\ddot{\underline{r}}_i - \ddot{\underline{r}}_0$ denotes the difference of accelerations between the satellite and the center of the Orbital Cartesian Coordinate System, $\underline{\rho}_i$ denotes the relative position vector of the i-th satellite, $\underline{\Omega}$ and $\dot{\underline{\Omega}}$ denote the angular velocity and angular acceleration vectors of the orbital CCS with respect to the inertial CCS. The dot symbol represent the time derivative in the inertial frame, and the circular symbol denotes the time derivative in the LVLH frame.
Thanks to the equation obtained, it is possible to directly integrate the relative dynamics, so as to impose a control of the relative position of the various satellites that make up the formation.
It is necessary to emphasize that in the considered case the center of the LVLH CCS does not represent a real satellite, but rather a virtual observer with respect to which the dynamics is described. It was chosen to consider on the chief only the perturbations due to the gravitational potential, considering harmonics up to J2.

$$\ddot{\underline{r}}_0 = \underline{a}_{g,0} \tag{3}$$

Where $\underline{a}_{g,0}$ represents the gravity acceleration acting on $\underline{r}_0$, calculated using earth gravitational potential using Legendre polynomial of order 2 and degree 0.
Thanks to this choice it is possible to introduce the equations described by Xu et al.[8], that gives an analytical formulation for the angular velocity $\underline{\Omega}$ and angular acceleration $\underline{\dot{\Omega}}$ of the orbital reference frame.
On the other hand, the accelerations that act on each body are:

$$\underline{\ddot{r}}_i = \underline{a}_{g,i} + \underline{a}_{d,i} + \underline{a}_{sp,i} + \underline{a}_{tb,i} + \underline{u}_i + \frac{1}{m_i}\sum_k \underline{t}_{k,i} \tag{4}$$

Where $\underline{a}_{g,i}$ represents the gravity acceleration acting on $\underline{r}_i$, calculated using earth gravitational potential using Legendre polynomial of order 4 and degree 4; $\underline{a}_{d,i}$ represents the atmospheric drag acceleration, taking into account the atmospheric density, calculated according to the Harris-Priester model [4], and the characteristics of the satellite; $\underline{a}_{sp,i}$ represent the solar radiation pressure acceleration, considering a shadow factor, the distance with respect to the Sun and the characteristics of the satellite; $\underline{a}_{tb,i}$ denotes the third body perturbation due to the Moon and the Sun, where both are modeled as point mass; m_i indicates the mass of the i-th body; $\underline{u}_i$ represents the control acceleration acting on the i-th satellite; finally, $\underline{t}_{k,i}$ refers to the tension force acting on the i-th body generated by the segment of tether that connects the i-th body to the k-th. These forces can be computed by considering the tether segments as one-directional springs. It is possible to define the tension in each tether segment as a function of orientation ($\hat{\tau}_{k,i}$), strain, and strain rate. By denoting the position of the spacecraft connected at the other end of the tether segment with $\underline{\rho}_k$, it is possible to indicate the direction of the tension as:

$$\hat{\tau}_{k,i} = \frac{\underline{\rho}_k - \underline{\rho}_i}{\|\underline{\rho}_k - \underline{\rho}_i\|} \tag{5}$$

The tension of the tether is:

$$\underline{t}_{k,i} = EA(\epsilon_{k,i} + c_{k,i}\dot{\epsilon}_{k,i})\hat{\tau}_{k,i} \tag{6}$$

Where E is the Young's modulus of the material composing the tether, A the cross section, $\epsilon_{k,i}$ the strain, $\dot{\epsilon}_{k,i}$ the strain rate, and $c_{k,i}$ the damping coefficient. In order to define the latter quantities, it is necessary to use the undeformed length of the tether $\bar{l}_{k,i}$, its mechanical stretch $\ell_{k,i}$ and its mechanical stretch rate $\dot{\ell}_{k,i}$ defined as:

$$\ell_{k,i} = \|\underline{\rho}_k - \underline{\rho}_i\| - \bar{l}_{k,i} \tag{7}$$

It is then possible to define:

$$\epsilon_{k,i} = \frac{\ell_{k,i}}{\bar{l}_{k,i}} \tag{8}$$

$$\dot{\epsilon}_{k,i} = \frac{\dot{\ell}_{k,i}}{\bar{l}_{k,i}} \tag{9}$$

The tension is represented graphically in Fig. 2. It is necessary to emphasize that, in contrast to what happens in a spring, in the case of the tether the tension forces are present only when the cable is stretched. In the case of compression, tethers instantly goes into a buckling, and the stress goes to 0. By subtracting Eq. 4 with Eq. 3, it yields:

$$\underline{\ddot{r}}_i - \underline{\ddot{r}}_0 = \Delta\underline{a}_{g,i} + \underline{a}_{d,i} + \underline{a}_{sp,i} + \underline{a}_{tb,i} + \underline{u}_i + \frac{1}{m_i}\sum_k \underline{t}_{k,i} \tag{10}$$

By substituting Eq. 10 in Eq. 2, the final expression of the equation of relative dynamics (Eq. 11) is derived.

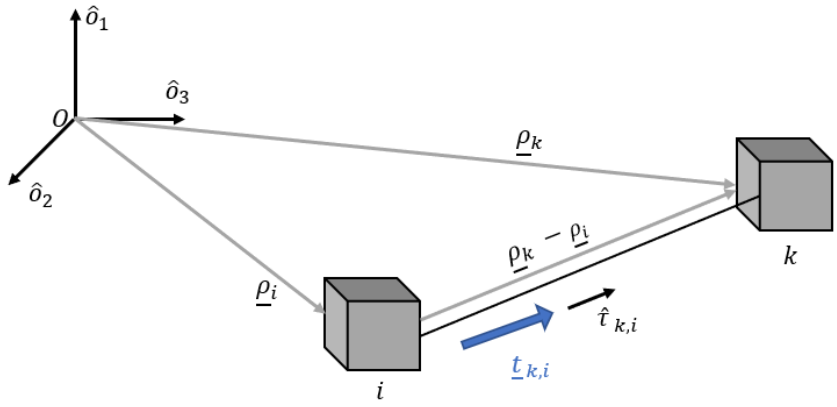

Figure 2: Description of the tether tension in LVLH components

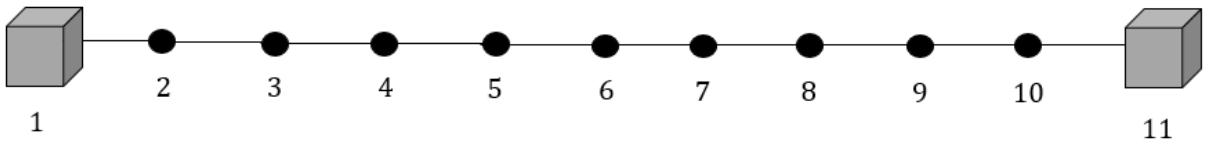

Figure 3: Schematisation of the system analysed in this study

$$\underline{\overset{\circ\circ}{\rho}}_i = \Delta\underline{a}_{g,i} + \underline{a}_{d,i} + \underline{a}_{sp,i} + \underline{a}_{tb,i} + \underline{u}_i + \frac{1}{m_i}\sum_k \underline{t}_{k,i} - \underline{\dot{\Omega}} \times \underline{\rho}_i - \underline{\Omega} \times \underline{\Omega} \times \underline{\rho}_i - 2\underline{\Omega} \times \underline{\overset{\circ}{\rho}}_i \tag{11}$$

At this point, the generic equation introduced can be applied to every body composing the system. In the case analysed, the system is composed of 11 different aligned bodies, that represents either satellites or lumps of tether. The first and the eleventh bodies represent the satellites at the extremities of the tether, the bodies relative to index between 2 and 10 represents lumps of tether, located at the center of mass of each segment (Fig. 3).

By using this model, a system of ordinary differential equation (ODE) is obtained, which considers 66 state variables. The state matrix is composed of the position components (3 states) and the velocity components (3 states) of every body composing the system. In order to obtain this set of 66 scalar ODE, the accelerations, the positions and the velocities are projected in scalar components on the LVLH CCS:

$$\boldsymbol{\rho}_i^L = \underline{\rho}_i \cdot \begin{Bmatrix} \hat{o}_1 \\ \hat{o}_2 \\ \hat{o}_3 \end{Bmatrix} = \begin{bmatrix} x_i \\ y_i \\ z_i \end{bmatrix}^L \quad \dot{\boldsymbol{\rho}}_i^L = \underline{\overset{\circ}{\rho}}_i \cdot \begin{Bmatrix} \hat{o}_1 \\ \hat{o}_2 \\ \hat{o}_3 \end{Bmatrix} = \begin{bmatrix} v_{xi} \\ v_{yi} \\ v_{zi} \end{bmatrix}^L \quad \ddot{\boldsymbol{\rho}}_i^L = \underline{\overset{\circ\circ}{\rho}}_i \cdot \begin{Bmatrix} \hat{o}_1 \\ \hat{o}_2 \\ \hat{o}_3 \end{Bmatrix} = \begin{bmatrix} \dot{v}_{xi} \\ \dot{v}_{yi} \\ \dot{v}_{zi} \end{bmatrix}^L \tag{12}$$

$$\mathbf{a}_i^L = (\Delta\underline{a}_{g,i} + \underline{a}_{d,i} + \underline{a}_{sp,i} + \underline{a}_{tb,i} - \underline{\dot{\Omega}} \times \underline{\rho}_i - \underline{\Omega} \times \underline{\Omega} \times \underline{\rho}_i - 2\underline{\Omega} \times \underline{\overset{\circ}{\rho}}_i) \cdot \begin{Bmatrix} \hat{o}_1 \\ \hat{o}_2 \\ \hat{o}_3 \end{Bmatrix} = \begin{bmatrix} a_{x,i} \\ a_{y,i} \\ a_{z,i} \end{bmatrix}^L \tag{13}$$

$$\mathbf{u}_i^L = \underline{u}_i \cdot \begin{Bmatrix} \hat{o}_1 \\ \hat{o}_2 \\ \hat{o}_3 \end{Bmatrix} = \begin{bmatrix} u_{x,i} \\ u_{y,i} \\ u_{z,i} \end{bmatrix}^L \tag{14}$$

$$\mathbf{t}_{k,i}^{L} = \underline{t}_{k,i} \cdot \begin{Bmatrix} \hat{o}_1 \\ \hat{o}_2 \\ \hat{o}_3 \end{Bmatrix} = \begin{bmatrix} (t_{k,i})_x \\ (t_{k,i})_y \\ (t_{k,i})_z \end{bmatrix}^{L} \tag{15}$$

Finally, Eq. 16 represents the ODE system used in the following analysis.

$$\begin{bmatrix} \dot{x}_1 \\ \dot{y}_1 \\ \dot{z}_1 \\ \dot{v}_{x1} \\ \dot{v}_{y_1} \\ \dot{v}_{z1} \\ \vdots \\ \dot{x}_i \\ \dot{y}_i \\ \dot{z}_i \\ \dot{v}_{xi} \\ \dot{v}_{y_i} \\ \dot{v}_{zi} \\ \vdots \\ \dot{x}_{11} \\ \dot{y}_{11} \\ \dot{z}_{11} \\ \dot{v}_{x11} \\ \dot{v}_{y_{11}} \\ \dot{v}_{z11} \end{bmatrix}^{L} = \begin{bmatrix} v_{x1} \\ v_{y_1} \\ v_{z1} \\ a_{x,1} + (t_{2,1})_x/m_1 + u_{x,1} \\ a_{y,1} + (t_{2,1})_y/m_1 + u_{y,1} \\ a_{z,1} + (t_{2,1})_z/m_1 + u_{z,1} \\ \vdots \\ v_{xi} \\ v_{y_i} \\ v_{zi} \\ a_{x,i} + (t_{i-1,i} + t_{i+1,i})_x/m_i \\ a_{y,i} + (t_{i-1,i} + t_{i+1,i})_y/m_i \\ a_{z,i} + (t_{i-1,i} + t_{i+1,i})_z/m_i \\ \vdots \\ v_{x11} \\ v_{y_{11}} \\ v_{z11} \\ a_{x,11} + (t_{10,11})_x/m_{11} + u_{x,11} \\ a_{y,11} + (t_{10,11})_y/m_{11} + u_{y,11} \\ a_{z,11} + (t_{10,11})_z/m_{11} + u_{z,11} \end{bmatrix}^{L} \tag{16}$$

Only one tension force is present on body 1 and 11, as these are connected only to the second and second-to-last satellites, respectively. In addition, the control accelerations act only on the satellites at the ends, so exclusively on bodies 1 and 11.
Finally, the states relative to the origin of the LVLH CCS are considered:

$$\begin{bmatrix} \dot{x}_0 \\ \dot{y}_0 \\ \dot{z}_0 \\ \dot{v}_{x0} \\ \dot{v}_{y_0} \\ \dot{v}_{z0} \end{bmatrix}^{E} = \begin{bmatrix} v_{x0} \\ v_{y_0} \\ v_{z0} \\ a_{x,0} \\ a_{y,0} \\ a_{z,0} \end{bmatrix}^{E} \tag{17}$$

In this case the ODE is propagated in ECI components.
By considering all the components, the final ODE system is composed of 72 states.

3 AERODYNAMIC-SURFACE MODELING

In this section the model used to simulate the aerodynamic surfaces controlling the systems is introduced. In order to produce the control force needed to keep the system in a formation, two flat plates are added to the satellites at the ends of the tether. These surfaces are placed in such a way to produce a lift force that keep a tension in the tether during the orbit (Fig. 4). The aerodynamic force generated by each surface can be decomposed into a lift component L, perpendicular to the orbital velocity, and

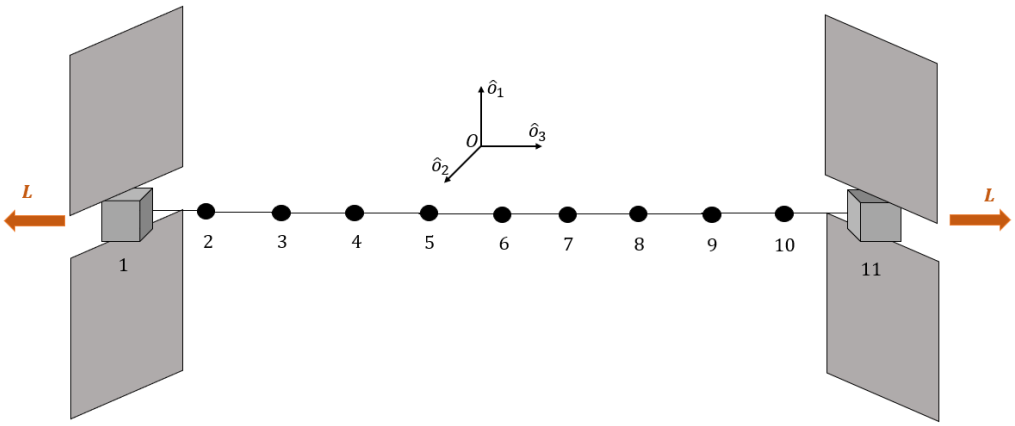

Figure 4: Representation of the system with stabilizing aerodynamic surfaces

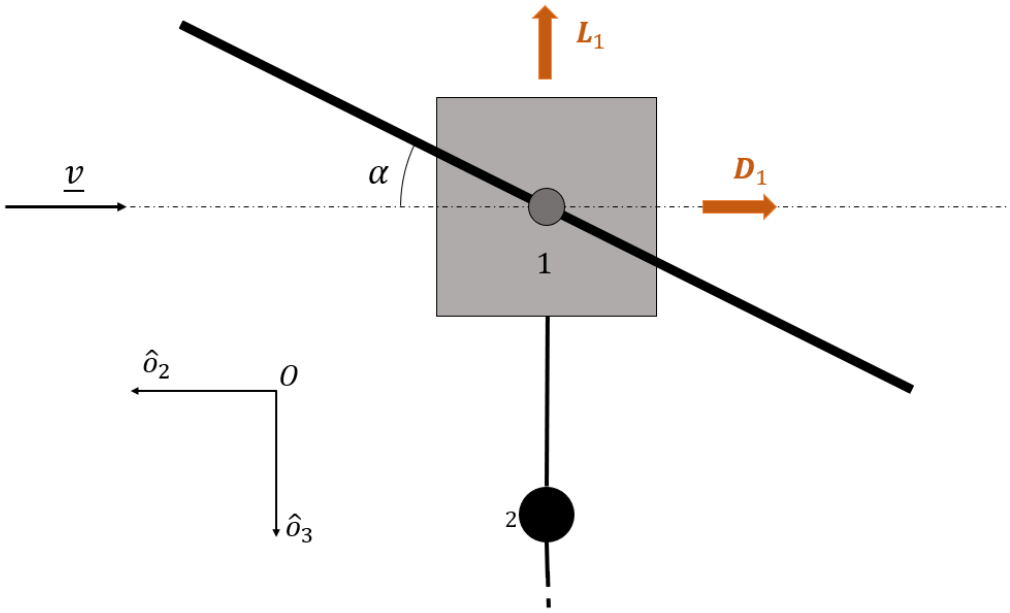

Figure 5: Satellite 1 view with representation of the aerodynamic forces generated by the flat plates

a drag component D, parallel to the velocity (Fig. 5).
These can be modeled as:

$$L = \frac{1}{2}\rho A \|\underline{v}\|^2 C_L \tag{18}$$

$$D = \frac{1}{2}\rho A \|\underline{v}\|^2 C_D \tag{19}$$

Where ρ denotes the atmospheric density, calculated according to the Harris-Priester model [4], A denotes a reference surface (in this case, the flat plate surface), $\underline{v}$ denotes the velocity with respect to the atmosphere, and C_L and C_D denote the coefficients of lift and drag of the plates, respectively. In order to obtain the aerodynamic coefficients of the surfaces as a function of the angle of attack α, the

free molecular flow model was used [5].

$$C_L = \left[\frac{2-\sigma_n-\sigma_t}{\sqrt{\pi}S}\exp\left(-S^2\sin^2\alpha\right)+\sigma_n\frac{v_w}{\|\underline{v}\|}\right]\sin 2\alpha + \left[\frac{2-\sigma_n}{S^2}+2(2-\sigma_n-\sigma_t)\sin^2\alpha\right]\cos\alpha\ \text{erf}(S\sin\alpha) \tag{20}$$

$$C_D = 2\sigma_n\frac{v_w}{\|\underline{v}\|}\sin^2\alpha+\frac{2}{\sqrt{\pi}S}\left[(2-\sigma_n)\sin^2\alpha+\sigma_t\cos^2\alpha\right]\exp\left(-S^2\sin^2\alpha\right)+ 2\left[(2-\sigma_n)\left(\sin^2\alpha+\frac{1}{2S^2}\right)+\sigma_t\cos^2\alpha\right]\sin\alpha\ \text{erf}(S\sin\alpha) \tag{21}$$

Where:

$$S=\frac{\|\underline{v}\|}{\sqrt{2RT}} \qquad v_w=\sqrt{\frac{\pi RT_w}{2}} \qquad \text{erf}(x)=\frac{2}{\sqrt{\pi}}\int_0^x e^{-t^2}dt \tag{22}$$

Denoting by T the atmospheric temperature, by T_w the temperature of the flat plates, R the specific gas constant, and σ_n and σ_t the tangential and normal reflective coefficients.

4 LINEARIZATION AND CONTROL

To control the tether system, an LQR controller was synthesized based upon a linearized model. In order to obtain a linearized model, a linearization analogous to that used by Quadrelli and Pastori was performed [6], [13], so as to obtain a dynamic equation of the type:

$$[\dot{\text{X}}] = [\text{A}][\text{X}] + [\text{B}][\text{F}]_{ctr} + [\text{L}][\text{F}]_{ext} \tag{23}$$

Where [A], [B] and [L] are, respectively, the state, input and disturbance matrices, $[\text{F}]_{ctr}$ and $[\text{F}]_{ext}$ represents respectively the column matrices of the control and external forces, and the state [X] is defined as:

$$[\text{X}] = \begin{bmatrix}\Delta\boldsymbol{\rho}_1^L\\ \Delta\boldsymbol{\rho}_{11}^L\\ \Delta\dot{\boldsymbol{\rho}}_1^L\\ \Delta\dot{\boldsymbol{\rho}}_{11}^L\end{bmatrix} = \begin{bmatrix}\boldsymbol{\rho}_1^L-\boldsymbol{\rho}_{1,eq}^L\\ \boldsymbol{\rho}_{11}^L-\boldsymbol{\rho}_{11,eq}^L\\ \dot{\boldsymbol{\rho}}_1^L-\dot{\boldsymbol{\rho}}_{1,eq}^L\\ \dot{\boldsymbol{\rho}}_{11}^L-\dot{\boldsymbol{\rho}}_{11,eq}^L\end{bmatrix} \tag{24}$$

The equilibrium state is considered in a cross-track configuration, i.e. with the tether parallel to the direction $\hat{o}_3$.

$$\tilde{\boldsymbol{\rho}}_{1,eq}^L = \begin{bmatrix}0\\0\\-l_{tether}/2\end{bmatrix}^L \quad \tilde{\boldsymbol{\rho}}_{11,eq}^L = \begin{bmatrix}0\\0\\l_{tether}/2\end{bmatrix}^L \quad \dot{\tilde{\boldsymbol{\rho}}}_{1,eq}^L = \dot{\tilde{\boldsymbol{\rho}}}_{11,eq}^L = \begin{bmatrix}0\\0\\0\end{bmatrix}^L \tag{25}$$

Where l_{tether} indicates the total length of the tether. Since it is intended to control only the relative position of the satellites, the equilibrium state is repositioned with respect to the current position and velocity of the centre of mass of the whole system:

$$[X]_{eq} = \begin{bmatrix}\boldsymbol{\rho}_{1,eq}^L\\ \boldsymbol{\rho}_{11,eq}^L\\ \dot{\boldsymbol{\rho}}_{1,eq}^L\\ \dot{\boldsymbol{\rho}}_{11,eq}^L\end{bmatrix} = \begin{bmatrix}\tilde{\boldsymbol{\rho}}_{1,eq}^L+\boldsymbol{\rho}_{CM}^L\\ \tilde{\boldsymbol{\rho}}_{11,eq}^L+\boldsymbol{\rho}_{CM}^L\\ \dot{\tilde{\boldsymbol{\rho}}}_{1,eq}^L+\dot{\boldsymbol{\rho}}_{CM}^L\\ \dot{\tilde{\boldsymbol{\rho}}}_{11,eq}^L+\dot{\boldsymbol{\rho}}_{CM}^L\end{bmatrix} \tag{26}$$

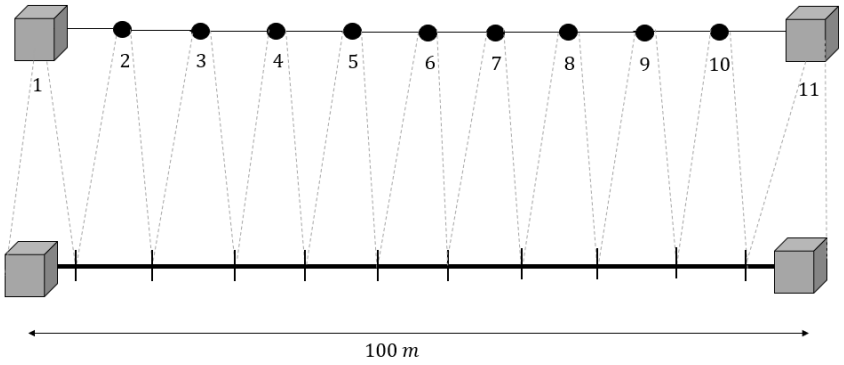

Figure 6: Representation of the discretization used

Where $\boldsymbol{\rho}_{CM}$ and $\dot{\boldsymbol{\rho}}_{CM}$ the position and velocity of the center of mass of the whole system.
By using the above mentioned matrices, the LQR control gain was computed by solving the Riccati equation:

$$-[\mathrm{Q}] - [\mathrm{A}]^T[\mathrm{P}]_\infty - [\mathrm{P}]_\infty[\mathrm{A}] + [\mathrm{P}]_\infty[\mathrm{B}][\mathrm{R}]^{-1}[\mathrm{B}]^T[\mathrm{P}]_\infty = 0 \tag{27}$$

$$[\mathrm{K}]_{LQR} = [\mathrm{R}]^{-1}[\mathrm{B}]^T[\mathrm{P}]_\infty = \begin{bmatrix}[\mathrm{K}]_{LQR,1} & [\mathrm{K}]_{LQR,11}\end{bmatrix} \tag{28}$$

Where $[\mathrm{K}]_{LQR,1}$ and $[\mathrm{K}]_{LQR,11}$ represent the gain matrices for the state feedback of the first and eleventh satellites, respectively.

5 SIMULATION SET-UP

The system analyzed in this study consists of two satellites connected by a tether with a length of 100 m. The data used for the tether characteristics are reported in Tab. 1. The tether are analogous to those used by Quadrelli and Lorenzini [1].

Table 1: Tether characteristics

Length	m	100
Linear Density	kg/km	10
Diameter	mm	1.7
Young Modulus	GPa	20.844
Axial Stiffness	N	47312
Damping	Ns	47.312

Considering the discretization used, the characteristics of the bodies are calculated. Given that the nine central bodies represent the centers of mass of a tether segments of 10 meters of length, and given the tether characteristics listed in the table above, the mass and surface values are calculated. The contribution of a half tether segment is also added to the satellites at the ends, as shown in the Fig. 6. The resulting values are shown in the Tab. 2.
The system is initialized in a cross-track configuration in LVLH coordinates, i.e., with all bodies at x and y null and z equispaced between -50 m and 50 m, so as to have the center of mass aligned with the center of the LVLH. The reference orbit, on which the LVLH is initialized, is circular, equatorial, with an altitude of 200 km.
For the aerodynamic surfaces placed on the end satellites, two square flat plates of 6 m^2 each are considered for each satellite. The characteristics of these surfaces are reported in Tab. 3.

Table 2: Satellites and tether lumps characteristics

		Satellite (i= 1,11)	Tether lumps (i= 2,3,4,5,6,7,8,9,10)
Mass	kg	50.05	0.1
Area (Spacecraft bus only)	m^2	1	0.017
Drag coefficient (Spacecraft bus only)	-	2	2
Reflectivity coefficient	-	1.1	1.1

Table 3: Aerodynamic surfaces characteristics

Total area for satellite	m^2	12
Normal reflective coefficient	-	0.7
Tangential reflective coefficient	-	0.7
Temperature	K	350

Finally, the control law was obtained using the weights described in Eq. 29.

$$[\mathrm{Q}] = \begin{bmatrix} [\mathrm{I}] & [0] \\ [0] & 10000[\mathrm{I}] \end{bmatrix} \quad [\mathrm{R}] = \frac{1}{F_{max}} \begin{bmatrix} [\mathrm{I}] & [0] \\ [0] & [\mathrm{I}] \end{bmatrix} \tag{29}$$

Where [I] and [0] are, respectively, 6 by 6 identity and zero matrices, and $F_{max} = 1\ N$ represents the maximal control value.

6 RESULTS

In this section the results of numerical simulations are reported, by considering the ODE system and the characteristics of the satellites and tether introduced above.
All plots show results in LVLH components referred to the center of mass of the system.
The first simulation performed considers the tether system positioned in a cross-track configuration, with no control applied (Eq. 30).

$$\mathbf{u}_1^L = \mathbf{u}_{11}^L = \begin{bmatrix} 0 \\ 0 \\ 0 \end{bmatrix}^L \tag{30}$$

In Fig. 7 the evolution of the system during half orbit can be observed.
The plot shows that the system is not stable, beginning to swing on the cross-track direction. This behaviour was to be expected, considering that the only stable configuration is radial, due to the gravitational gradient.
At this point the LQR controller is introduced (Eq. 31), applying the control accelerations on the satellites at the end of the tether, obtained with control gains introduced in Eq. 28.

$$\mathbf{u}_1^L = \frac{[\mathrm{K}]_{LQR,1}}{m_1} \begin{bmatrix} x_1 - x_{1,eq} \\ y_1 - y_{1,eq} \\ z_1 - z_{1,eq} \\ v_{x1} - v_{x1,eq} \\ v_{y_1} - v_{y1,eq} \\ v_{z1} - v_{z1,eq} \end{bmatrix}^L = \begin{bmatrix} u_{x,1} \\ u_{y,1} \\ u_{z,1} \end{bmatrix}^L \quad \mathbf{u}_{11}^L = \frac{[\mathrm{K}]_{LQR,11}}{m_{11}} \begin{bmatrix} x_{11} - x_{11,eq} \\ y_{11} - y_{11,eq} \\ z_{11} - z_{11,eq} \\ v_{x11} - v_{x11,eq} \\ v_{y11} - v_{y11,eq} \\ v_{z11} - v_{z11,eq} \end{bmatrix}^L = \begin{bmatrix} u_{x,11} \\ u_{y,11} \\ u_{z,11} \end{bmatrix}^L \tag{31}$$

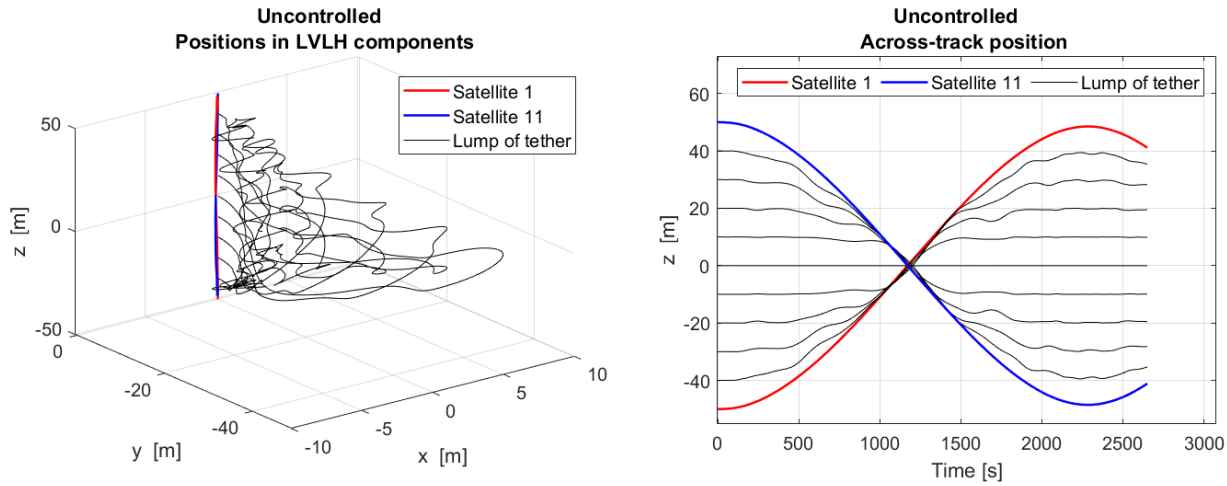

Figure 7: Simulation of an uncontrolled system initialized in a cross-track configuration

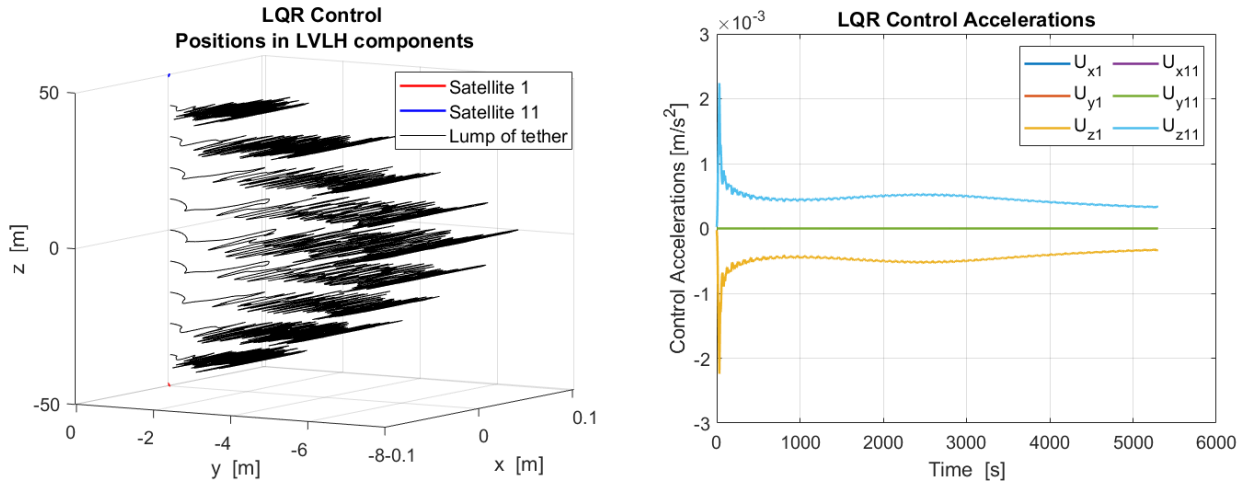

Figure 8: Simulation of a controlled orbit using LQR controller

In this case, the system maintains the desired configuration (Fig. 8). Oscillations of the lumps of tether on the order of few meters can be seen, as the tether tends to arch due to aerodynamic drag. Despite this, the satellites maintain their reference position, oscillating only of a few centimeters. By analyzing the applied control accelerations, it can be noticed that the only significant component is in the cross-track direction, and opposite for the two satellites.
An additional simulation introduced a control on the system only in this direction, to test whether this is sufficient to keep the system in formation. To do this, constant, opposing control accelerations are introduced for the two satellites, constantly tensioning the tether (Eq. 32). The value of the control acceleration used was extrapolated from the average value of the previous simulation.

$$\mathbf{u}_1^L = \begin{bmatrix} 0 \\ 0 \\ -5 \cdot 10^{-4} \end{bmatrix}^L \text{ms}^{-2} \qquad \mathbf{u}_{11}^L = \begin{bmatrix} 0 \\ 0 \\ 5 \cdot 10^{-4} \end{bmatrix}^L \text{ms}^{-2} \tag{32}$$

Fig. 9 shows the results of this simulation. The stabilization achieved with constant, unidirectional control accelerations provides performance similar to that achieved with an active control, by keeping the system close to the nominal configuration.
The last simulation considers the system with aerodynamic surfaces. As presented earlier, these are arranged in such a way as to generate a lift in the cross-track direction on the two end satellites, so as

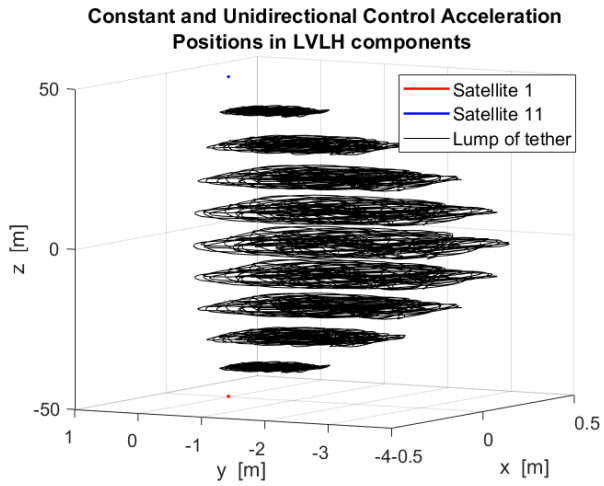

Figure 9: Simulation of a controlled orbit using constant and unidirectional control acceleration

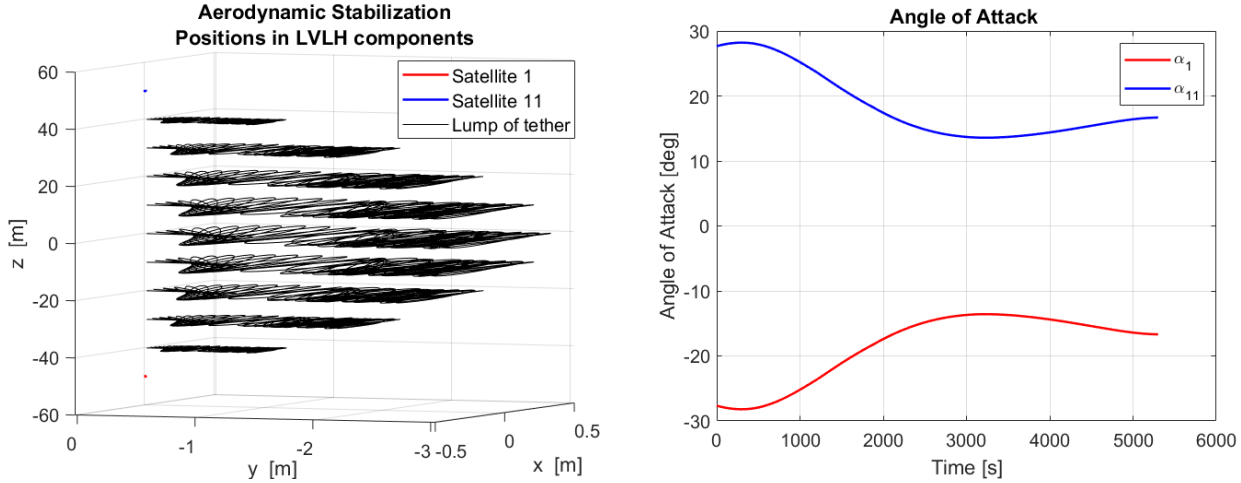

Figure 10: Simulation of a controlled orbit using aerodynamic stabilization

to provide the tension needed to maintain the system in the desired configuration (Eq. 33).

$$\mathbf{u}_1^L = \frac{1}{m_1}\begin{bmatrix} 0 \\ -D_1 \\ L_1 \end{bmatrix}^L \qquad \mathbf{u}_{11}^L = \frac{1}{m_{11}}\begin{bmatrix} 0 \\ -D_{11} \\ L_{11} \end{bmatrix}^L \tag{33}$$

In this stabilization, the angle of attack was calculated to ensure a constant lift equal to the value used in the previous simulation, by considering the velocity of the system with respect to the atmosphere and the change in density. Figs. 10 and 11 show the evolution of the position of the bodies during an orbit, the angle of attack of the aerodynamic surfaces of the two satellites, and the aerodynamic accelerations generated.

The angle of attack varies continuously to ensure a constant lift, by compensating for the effects of variation of the aerodynamic density. The main causes of density variation are due to Harris-Priester model [4], which takes into account density fluctuations by considering the effect of solar radiation, and the increase of the density due to the decrease in altitude caused by the atmospheric drag.

Despite the drag acting on both satellites, the lift generated by the aerodynamic surfaces succeeds in keeping the system in the desired configuration. It is consequently shown that such a system is able to stabilize in cross-track configuration using only aerodynamic effects.

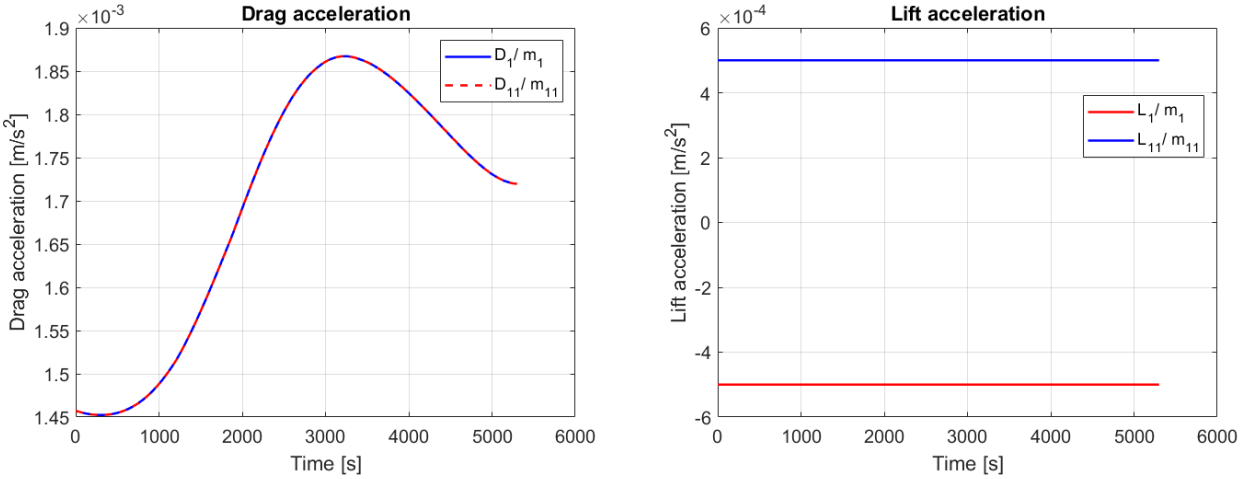

Figure 11: Lift and Drag acceleration produced by the aerodynamic stabilization

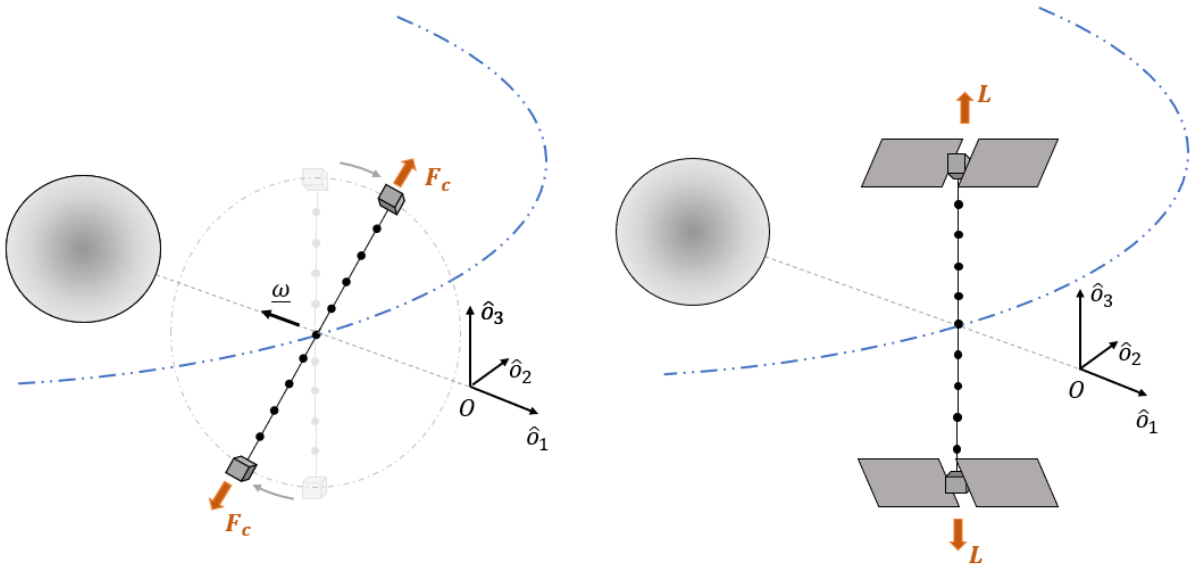

Figure 12: Comparison of the aerodynamic stabilization proposed (right) and a gyroscopic stabilization (left)

7 COMPARISON WITH A GYROSCOPIC STABILIZATION

In this section, the aerodynamic stabilization analyzed in this paper is compared with a stabilization strategy which utilizes the gyroscopic effect to generate the tension in the tether. A representation of these two types of stabilization can be seen in the Fig. 12.

As shown graphically in the figure, gyroscopic stabilization consists of putting the system into rotation so as to generate a constant tension in the tether, ensuring a periodic oscillation in the cross-track direction ($\hat{o}_3$). The rotational speed can be modulated according to the needs of the mission, but this will still have an bottom limit due to the minimum stabilization tension and top limit defined by the mechanical characteristics of the tether.

Although these two stabilization methodologies are very different, both allow the achievement of a system that extends in the cross-track direction during an orbit, even if with different behaviors (Fig. 13). The aerodynamically stabilized system provides a constant distribution of satellites in the z-direction, thus ensuring a constant cross-track base-line throughout the mission. As mentioned earlier, this kind of configuration would maximize performance in terms of remote sensing for earth

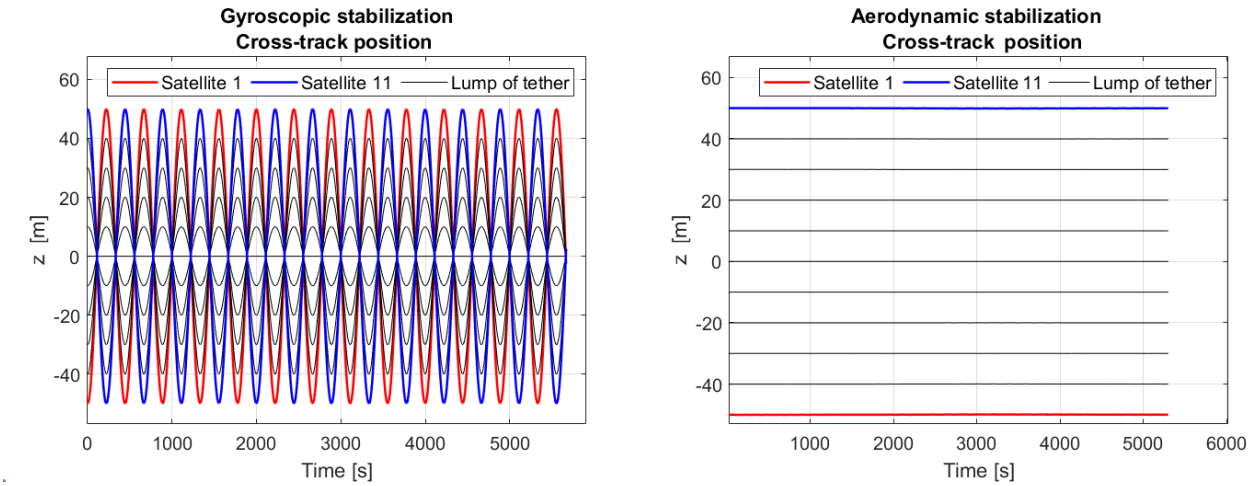

Figure 13: Comparison of the cross-track projection for the two proposed stabilizations

observations. Nevertheless, it must be emphasized that the aerodynamic surfaces required for stabilization in combination with the LEO's dense atmosphere generate significant drag, which de-orbit the system quickly, consequently requiring frequent maneuvers to restore the system to its reference orbit. A gyroscopic stabilization, on the other hand, does not require the atmosphere for proper operation, finding possible applications even in environments other than low Earth orbit. In addition, a gyroscopically stabilized system requires far fewer corrections to maintain orbit and reference configuration. However, its angular velocity is nominally aligned in the inertial frame, possibly making more complicated the remote sensing operations, and the continuous oscillations in the cross-track direction generate quite a few constraints for the mission. Since the system has to exploit the period of maximum extension in the cross-track direction to make the measurement, there will be constraints in terms of acquisition duration and time interval between acquisitions.

8 CONCLUSIONS

In this paper, an aerodynamic control technique applied to tether satellite systems was analyzed. Through the introduction of a control law, it was possible to demonstrate, by simulations, that it is possible to maintain a tether system in a cross-track configuration through a constant control acceleration applied on the end satellites. By maintaining a constant tension in the tether, in fact, it is possible to ensures the positioning of the satellites in the formation, because the tether generates an elastic pullback force when they move from their equilibrium position. The introduction of aerodynamic surfaces on the end satellites was considered, so as to generate the tensions in the tether by aerodynamic lift. Despite the advantage of this stabilization, however, it is necessary to consider the drawbacks caused by aerodynamic drag. In order to function properly, this configuration needs to be in very low orbit, where aerodynamic drag has a considerable effect on satellites, causing a fast orbit decay. Possible solutions could be a mission optimization or the combination of stabilizing surfaces and air-breathing electric motors, which could ensure continuous propulsion of the system during the mission, continuously compensating for the effects of aerodynamic drag.

9 ACKNOWLEDGMENT

Dr. Quadrelli's contribution was carried out at the Jet Propulsion Laboratory, California Institute of Technology, under a contract with the National Aeronautics and Space Administration (80NM0018D0004), as part of the JPL Visiting Student Research Program that hosted Mr. Aliberti

under the mentorship of Dr. Quadrelli. This paper contains significant new information with respect to the initial work performed by Mr. Aliberti during the internship with JPL under the supervision of Dr. Quadrelli. In particular, the method for the stabilization of a cross-track tether satellite system by sole use of aerodynamic surfaces, introduced in this paper, is new and was developed after Mr. Aliberti in November 2022 became a Ph.D. candidate at Politecnico di Torino, under the advisorship of Prof. Marcello Romano.

REFERENCES

[1] M. Quadrelli and E. Lorenzini, "Dynamics and stability of a tethered centrifuge in low earth orbit," *Journal of the Astronautical Sciences*, vol. 40, 1992.

[2] S. Singh and W. Yim, "Feedback linearization and solar pressure satellite attitude control," *IEEE Transactions on Aerospace and Electronic Systems*, vol. 32, no. 2, pp. 732–741, 1996. DOI: 10.1109/7.489516.

[3] M. L. Cosmo and E. C. Lorenzini, "Tethers in space handbook," Tech. Rep., 1997.

[4] O. Montenbruck, E. Gill, and F. Lutze, "Satellite Orbits: Models, Methods, and Applications," *Applied Mechanics Reviews*, vol. 55, no. 2, B27–B28, Apr. 2002, ISSN: 0003-6900. DOI: 10.1115/1.1451162.

[5] J. Storch, "Aerodynamic disturbances on spacecraft in free-molecular flow," Aerospace corp el segundo ca vehicle systems div, Tech. Rep., 2002.

[6] M. B. Quadrelli, "Effect of distributed rod and string flexibility on formation dynamic stability," *The Journal of the astronautical sciences*, vol. 51, pp. 339–357, 2003. DOI: 10.1007/BF03546302.

[7] R. Bevilacqua and M. Romano, "Rendezvous maneuvers of multiple spacecraft using differential drag under j2 perturbation," *Journal of Guidance, Control, and Dynamics*, vol. 31, no. 6, pp. 1595–1607, 2008. DOI: 10.2514/1.36362.

[8] G. Xu and D. Wang, "Nonlinear dynamic equations of satellite relative motion around an oblate earth," *Journal of Guidance, Control, and Dynamics*, vol. 31, no. 5, pp. 1521–1524, 2008. DOI: 10.2514/1.33616.

[9] Y. Chen, R. Huang, L. He, X. Ren, and B. Zheng, "Dynamical modelling and control of space tethers: A review of space tether research," *Nonlinear Dynamics*, vol. 77, pp. 1077–1099, 2014. DOI: 10.1007/s11071-014-1390-5.

[10] S. Chesi, Q. Gong, and M. Romano, "Aerodynamic three-axis attitude stabilization of a spacecraft by center-of-mass shifting," *Journal of guidance, control, and dynamics*, vol. 40, no. 7, pp. 1613–1626, 2017. DOI: 10.2514/1.G002460.

[11] L. Carrer, C. Gerekos, F. Bovolo, and L. Bruzzone, "Distributed radar sounder: A novel concept for subsurface investigations using sensors in formation flight," *IEEE Transactions on Geoscience and Remote Sensing*, vol. 57, no. 12, pp. 9791–9809, 2019. DOI: 10.1109/TGRS.2019.2929422.

[12] A. D. Ogundele and M. Romano, "Dynamics and control of a cross-track-lift (ctrl) tethered spacecraft system," Spacecraft Robotics Laboratory, Naval Postgraduate School, Monterey, California, 93940, Tech. Rep., Jun. 2019.

[13] M. Pastori, F. Braghin, M. B. Quadrelli, and R. Beauchamp, "Modeling, dynamics and control of a variable topology tethered space system," in *2022 IEEE Aerospace Conference (AERO)*, 2022, pp. 1–20. DOI: 10.1109/AERO53065.2022.9843490.